



# Acid strength and solvation effects on methylation, hydride transfer, and isomerization rates during catalytic homologation of C<sub>1</sub> species

Dante A. Simonetti<sup>a</sup>, Robert T. Carr<sup>a</sup>, Enrique Iglesia<sup>a,b,\*</sup>

<sup>a</sup> Department of Chemical and Biomolecular Engineering, University of California at Berkeley, USA

<sup>b</sup> Division of Chemical Sciences, E.O. Lawrence Berkeley National Laboratory, Berkeley, CA 94720, USA

## ARTICLE INFO

### Article history:

Received 12 May 2011

Revised 6 September 2011

Accepted 6 September 2011

Available online 26 October 2011

### Keywords:

Dimethyl ether  
Solid acid catalysis  
Acid strength  
Confinement effects  
Zeolites  
Carbenium ion  
Homologation

## ABSTRACT

Dimethyl ether (DME) homologation forms isobutane and triptane (2,2,3-trimethylbutane) with supra-equilibrium selectivities within C<sub>4</sub> and C<sub>7</sub> hydrocarbons on both mesoporous solid acids (SiO<sub>2</sub>–Al<sub>2</sub>O<sub>3</sub>, H<sub>3</sub>PW<sub>12</sub>O<sub>40</sub>/SiO<sub>2</sub>) and the acid forms of various zeolites (BEA, FAU, MFI) via methylation and hydride transfer steps that favor isobutane and triptane formation because of the relative stabilities of ion-pairs at transition states for chains along the preferred growth path. The stabilities of ion-pair transition states increase as acid sites become stronger and energies for charge separation decrease and as van der Waals interactions within pores become stronger, which respectively lead to higher rates on H<sub>3</sub>PW<sub>12</sub>O<sub>40</sub>/SiO<sub>2</sub> and aluminosilicate zeolites than on amorphous SiO<sub>2</sub>–Al<sub>2</sub>O<sub>3</sub>. Solid acids with different strengths and abilities to solvate ion-pairs by confinement differ in selectivity because strength and solvation influence transition states for the hydride transfer, methylation, and isomerization steps to different extents. Stronger acid sites on H<sub>3</sub>PW<sub>12</sub>O<sub>40</sub>/SiO<sub>2</sub> favor isomerization and hydride transfer over methylation; they lead to higher selectivities to *n*-butane and non-triptane C<sub>7</sub> isomers than the weaker acid sites on BEA, FAU, and mesoporous SiO<sub>2</sub>–Al<sub>2</sub>O<sub>3</sub>. This preference for hydride transfer and isomerization on stronger acids reflects transition states with more diffuse cationic charge, which interact less effectively with conjugate anions than more localized cations at methylation transition states. The latter recover a larger fraction of the energy required to form the ion-pair, and their stabilities are less sensitive to acid strength than for diffuse cations. Large-pore zeolites (BEA, FAU) form triptane with higher selectivity than SiO<sub>2</sub>–Al<sub>2</sub>O<sub>3</sub> because confinement within large pores preferentially solvates the larger transition states for hydride transfer and methylation, which preserve the four-carbon backbone in triptane, over smaller transition states for alkoxide isomerization steps, which disrupt this backbone and cause growth beyond C<sub>7</sub> chains and subsequent facile β-scission to form isobutane. MFI forms isobutane and triptane with much lower selectivity than mesoporous acids or large-pore zeolites, because smaller pores restrict the formation of bimolecular methylation and hydride transfer transition states required for chain growth and termination steps to a greater extent than those for monomolecular alkoxide isomerization. These data and their mechanistic interpretations show that the selective formation of isobutane and triptane from C<sub>1</sub> precursors like DME is favored on all acids as a result of the relative stability of methylation, hydride transfer, and isomerization transition states, but to a lesser extent when small confining voids and stronger acid sites preferentially stabilize monomolecular isomerization transition states. The observed effects of acid strength and confinement on rates and selectivities reflect the more effective stabilization of all ion-pairs on stronger acids and within solvating environments, but a preference for transition states with more diffuse charge on stronger acids and for ion-pairs with the appropriate solvation within voids of molecular dimensions.

© 2011 Elsevier Inc. All rights reserved.

## 1. Introduction

Recent studies have demonstrated the selective synthesis of triptyl species (2,2,3-trimethylbutane and 2,3,3-trimethyl-1-butene; -tyl

used here and throughout to define alkenes and alkanes with a given backbone structure) and isobutyl species from methanol or dimethyl ether (DME) via Brønsted acid-catalyzed pathways mediated by carbenium ion transition states. This reaction occurs at modest temperatures (400–500 K) in liquid-phase metal–halogen systems [1–5] and on zeolites in their acid forms (H-FER, H-MOR, H-MFI, H-FAU, H-BEA) [6]. Competitive reactions between <sup>13</sup>C-labeled dimethyl ether (<sup>13</sup>C-DME) and unlabeled alkenes on BEA,

\* Corresponding author at: Department of Chemical and Biomolecular Engineering, University of California at Berkeley, USA. Fax: +1 510 642 4778.

E-mail addresses: [iglesia@cchem.berkeley.edu](mailto:iglesia@cchem.berkeley.edu), [iglesia@berkeley.edu](mailto:iglesia@berkeley.edu) (E. Iglesia).

the zeolite that showed the highest triptane selectivity (21% C<sub>7</sub> species; 72% triptyls within C<sub>7</sub>) [7], led to the detailed reaction network shown in Scheme 1.

Chain growth occurs via methylation events that avoid primary carbocationic transition states such that C<sub>1</sub> species add to alkenes at positions that retain a four-carbon backbone. Chains terminate via hydride transfer reactions at rates dictated by the strength of the C–H bonds in the hydride donor molecules and by the stability of the carbenium ions formed as transition states during hydride transfer to alkoxide acceptors [7–10]. Methylation is fast relative to hydride transfer for chains along the preferred methylation path, but hydride transfer to 2,3,3-trimethyl *sec*-butoxide (the alkoxide precursor to triptane) is faster than triptene methylation. Chains terminate preferentially as triptane or isobutane because the tertiary carbenium ion transition states involved in hydride transfer to their alkoxides are more stable than those with primary character required for methylation of triptene or isobutene. The formation of alkanes requires that arenes be concurrently formed to satisfy the hydrogen stoichiometry of methanol and DME homologation to these saturated products [2,6,7,11]. Slow isomerization and  $\beta$ -scission of the alkoxide isomers preferentially formed along the chain growth path to triptane prevent backbone rearrangement or cleavage during chain growth. Methylation at less preferred positions forms species that rapidly grow to chains larger than C<sub>7</sub> (C<sub>8+</sub>), which undergo facile  $\beta$ -scission to form isobutene and isobutane. These mechanistic features of C<sub>1</sub> homologation and the resulting isomer and chain size distributions reflect the selective formation of the most highly substituted carbenium ions at transition states of elementary steps (i.e. methylation, termination, isomerization, and  $\beta$ -scission) involved in chain growth pathways [2,5–7].

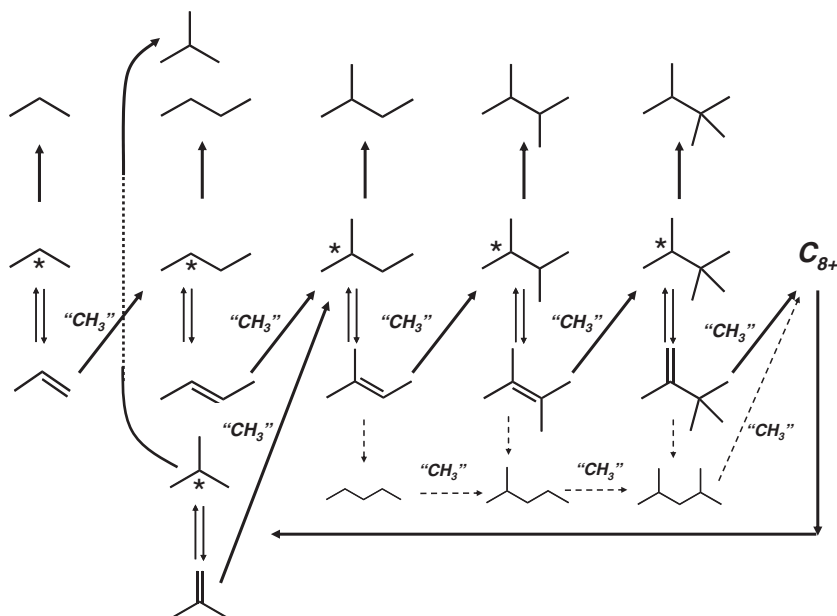
Here, we present data for DME homologation on acids with different spatial constraints but similar acid strength (mesoporous SiO<sub>2</sub>–Al<sub>2</sub>O<sub>3</sub> and zeolites BEA, FAU, and MFI), as well as on stronger acids on mesoporous supports (H<sub>3</sub>PW<sub>12</sub>O<sub>40</sub>/SiO<sub>2</sub>) to probe how spatial confinement and acid strength influence the rates of the various steps involved in acid-catalyzed homologation. These data and their mechanistic interpretation show that isomerization and hydride transfer rates are more sensitive to acid strength than methylation and that zeolites have higher rates of acid-catalyzed

reactions than mesoporous SiO<sub>2</sub>–Al<sub>2</sub>O<sub>3</sub>, because transition states confined within zeolite channels are stabilized with respect to gas-phase reactants by van der Waals interactions. DME homologation on medium-pore zeolites leads to a broad distribution of hydrocarbon chain lengths instead of the bimodal distribution to C<sub>4</sub> and C<sub>7</sub> products observed on large-pore zeolites because smaller pores hinder the formation of monomolecular isomerization transition states to a lesser extent than those for methylation and hydride transfer steps. These data give insights into the respective roles of solvation and acid strength on methylation, hydride transfer, isomerization, and  $\beta$ -scission rates and rigorously assess these effects using stabilities of the carbenium ion transition states that mediate these reactions.

## 2. Experimental methods

### 2.1. Catalysts, reactants, and kinetic and isotopic tracer studies

The acid forms of zeolites BEA, MFI, and FAU were prepared by heating NH<sub>4</sub>-BEA (Si/Al = 12.5, Zeolyst), NH<sub>4</sub>-MFI (Si/Al = 15, Zeolyst), and NH<sub>4</sub>-FAU (Si/Al = 3.2) to 773 K (at 0.02 K s<sup>-1</sup>) for 10 h in flowing dry air (1.7 cm<sup>3</sup> s<sup>-1</sup> g<sup>-1</sup>, zero grade, Praxair). NH<sub>4</sub>-FAU was prepared by treating NH<sub>4</sub>-Y zeolite with ammonium hexafluorosilicate solutions, using procedures described previously [12,13]. H<sub>3</sub>PW<sub>12</sub>O<sub>40</sub>/SiO<sub>2</sub> was prepared via incipient wetness impregnation of mesoporous SiO<sub>2</sub> (Cab-O-Sil HS-5; 310 m<sup>2</sup> g<sup>-1</sup>; 1.5 cm<sup>3</sup> g<sup>-1</sup> pore volume) with a solution of H<sub>3</sub>PW<sub>12</sub>O<sub>40</sub> (Sigma-Aldrich; reagent grade) in ethanol (Sigma-Aldrich; >99.5%; anhydrous) [14] to give samples with a 5% weight loading (5 wt.%). At this surface density, H<sub>3</sub>PW<sub>12</sub>O<sub>40</sub> species exist as isolated clusters or small two-dimensional aggregates on SiO<sub>2</sub> and have Keggin structure, as shown by MAS-<sup>31</sup>P NMR spectra and transmission electron micrographs [14]. Mesoporous SiO<sub>2</sub>–Al<sub>2</sub>O<sub>3</sub> (Si/Al = 5.7; Sigma-Aldrich) was used as received. DME homologation rates on each catalyst are normalized by the number of Brønsted acid sites (i.e., accessible protons) in each catalyst as measured from the number of 2,6-di-*tert*-butylpyridine molecules required to completely suppress methanol dehydration rates, assuming a 1:1 titrant:H<sup>+</sup> adsorption stoichiometry [14].



**Scheme 1.** Chain growth sequence for dimethyl ether homologation (starting with propene for simplicity). The asterisk indicates the preferred position of alkoxide attachment to the surface. “CH<sub>3</sub>” represents surface methylating species derived from dimethyl ether [1,6,7].

Rate data were obtained using quartz (12.5 mm OD) or stainless steel (9.5 mm OD) plug-flow reactors containing catalyst samples (0.14–0.28 g; 180–250  $\mu\text{m}$  particles) held onto a porous quartz disk or quartz wool. Samples were heated to 773 K (at 0.02 K s<sup>-1</sup>), held for 2 h in flowing dry air (0.8 cm<sup>3</sup> s<sup>-1</sup>, zero grade, Praxair), and then cooled to 473 K. Temperatures were controlled electronically (Watlow, Series 989) and measured with a type-K thermocouple held at the external reactor wall. Ar (0.8 cm<sup>3</sup> s<sup>-1</sup>, UHP, Praxair) was used to remove residual air from the reactor before introducing reactants consisting of DME (0.08–0.17 cm<sup>3</sup> s<sup>-1</sup>, 99.5%, Matheson), Ar (0.025–0.05 cm<sup>3</sup> s<sup>-1</sup>, 99.999%, Praxair), and propene (0.008–0.017 cm<sup>3</sup> s<sup>-1</sup> of 20% propene (99.999% purity), 5% Ar, 75% He; Praxair). Gaseous reactants were metered with electronic mass flow controllers (Porter, Model 201). The reactor effluent was transferred via heated lines (>373 K) into a gas chromatograph (Agilent 6890) equipped with a dimethylpolysiloxane column (HP-1, 50 m  $\times$  0.32 mm  $\times$  1.05  $\mu\text{m}$ ) connected to a flame ionization detector for chemical composition analysis.

Rate data with <sup>13</sup>C-labeled dimethyl ether (<sup>13</sup>C-DME) and <sup>12</sup>C-2,3-dimethyl-2-butene (98%, Sigma–Aldrich) were measured in a stainless steel plug-flow reactor (6.4 mm OD) containing the catalyst samples (0.03–0.07 g; 180–250  $\mu\text{m}$  particles) held onto a fritted gasket by quartz wool. Samples were heated to reaction temperature (473 K at 0.08 K s<sup>-1</sup>) in flowing He (0.08 cm<sup>3</sup> s<sup>-1</sup>, UHP, Praxair). The reactor effluent was transferred via heated lines (>373 K) into a gas chromatograph equipped with flame ionization and mass-selective detectors (Agilent 7890A/5975C), each connected to a capillary column (HP-1, dimethylpolysiloxane, 50 m  $\times$  0.32 mm  $\times$  1.05  $\mu\text{m}$ ) to measure chemical and isotopic compositions. Isotopic compositions and isotopologue distributions (see Supporting information) were determined from mass fragmentation patterns using deconvolution methods reported previously [15].

## 2.2. Determination of rates of methylation, hydride transfer, isomerization, and $\beta$ -scission of C<sub>8+</sub> species from isotopic tracer studies

Reactions of <sup>13</sup>C-DME with unlabeled alkenes were used in previous studies [7] to determine individual rates of methylation, hydride transfer, isomerization, and  $\beta$ -scission of intermediates formed during homologation of C<sub>1</sub> species on BEA. Here, as in previous studies, reactions of <sup>13</sup>C-DME with <sup>12</sup>C-2,3-dimethyl-2-butene were used to measure the individual rates of methylation of 2,3-dimethyl-2-butene and of hydride transfer and isomerization of 2,3-dimethyl *sec*-butoxide on the zeolites described in Section 2.1 and H<sub>3</sub>PW<sub>12</sub>O<sub>40</sub>/SiO<sub>2</sub> (further calculation details in the Supporting information). These rates were used to determine chain termination ( $\beta$ ) and skeletal isomerization ( $\gamma_{\text{sk}}$ ) probabilities, defined as the ratio of the rates of hydride transfer and isomerization, respectively, to the sum of hydride transfer and methylation rates (see Supporting information) [7].

Methylation of <sup>12</sup>C-2,3-dimethyl-2-butene by <sup>13</sup>C-DME form C<sub>8+</sub> chains that can undergo subsequent methyl shift isomerization (without backbone rearrangement) and  $\beta$ -scission to form isobutane and isobutene, the latter of which can re-enter homologation paths via methylation with <sup>13</sup>C-DME [7]. <sup>12</sup>C-2,3-dimethyl-2-butene molecules that form C<sub>8+</sub> chains and undergo  $\beta$ -scission appear as <sup>12</sup>C atoms in C<sub>1</sub>–C<sub>5</sub> molecules and as C<sub>6+</sub> homologation products with binomial distributions of <sup>12</sup>C-atoms [16]. Formation rates of species containing at least one <sup>12</sup>C-atom ( $R_{\text{Me}}$ ), but excluding rates of hydride transfer ( $R_{\text{HT}}$ ) and isomerization ( $R_{\text{Is}}$ ), are determined from isotopologue distributions as described previously [7,16] and in the Supporting information. The rate of  $\beta$ -scission of C<sub>8+</sub> chains ( $R_{\beta\text{s}}$ ) is given by:

$$R_{\beta\text{s}} = R_{\text{Me}} - R_{13\text{C}_1\text{-triptane}} \quad (1)$$

in which  $R_{13\text{C}_1\text{-triptane}}$  represents the rate of formation of singly labeled triptyl species (triptane and triptene). The sum of the rates of formation of singly labeled triptyls ( $R_{13\text{C}_1\text{-triptane}}$ ), hydride transfer ( $R_{\text{HT}}$ ), and isomerization ( $R_{\text{Is}}$ ) represents the rate at which species derived from <sup>12</sup>C-2,3-dimethyl-2-butene molecules terminate before forming C<sub>8+</sub> chains and undergoing  $\beta$ -scission. Thus, the  $\beta$ -scission probability of C<sub>8+</sub> chains ( $\gamma_{\beta\text{s}}$ ; Eq. (2)) represents the ratio of the rate of C<sub>8+</sub> chains (originating from <sup>12</sup>C-dimethyl-2-butene molecules) that undergo  $\beta$ -scission (Eq. (1)) to the formation rate of species (originating from <sup>12</sup>C-dimethyl-2-butene molecules) that terminate before  $\beta$ -scission.

$$\gamma_{\beta\text{s}} = \frac{R_{\beta\text{s}}}{R_{13\text{C}_1\text{-triptane}} + R_{\text{HT}} + R_{\text{Is}}} \quad (2)$$

## 3. Results and discussion

Catalytic homologation of DME (70–85 kPa) was carried out using streams containing small propene concentrations (1.8–2.0 kPa) to avoid induction periods caused by the slow formation of the first C–C bond from C<sub>1</sub> reactants as shown in previous studies [17]. These reactions were carried out on large-pore zeolites (BEA, FAU), a medium-pore zeolite (MFI), and mesoporous acids (SiO<sub>2</sub>–Al<sub>2</sub>O<sub>3</sub>, 5 wt.% H<sub>3</sub>PW<sub>12</sub>O<sub>40</sub>/SiO<sub>2</sub>) to probe the effects of acid strength and solvation by confinement on DME homologation rates and selectivities.

We examine the effects of acid strength first by comparing homologation rates and selectivities on 5 wt.% H<sub>3</sub>PW<sub>12</sub>O<sub>40</sub>/SiO<sub>2</sub> to those on SiO<sub>2</sub>–Al<sub>2</sub>O<sub>3</sub> and BEA (Section 3.1), because Brønsted acid sites on H<sub>3</sub>PW<sub>12</sub>O<sub>40</sub> Keggin clusters are much stronger than those in zeolites and SiO<sub>2</sub>–Al<sub>2</sub>O<sub>3</sub>, as shown from their respective deprotonation energies (DPE). DPE, a rigorous measure of acid strength derived from *ab initio* calculations for solid acids with well-defined inorganic structures [18,19], reflects the energy needed to remove a proton and separate it to non-interacting distances from the conjugate anion. DPE values depend on the stability of the anion formed and on the energy required to overcome the electrostatic interactions between the proton and the anion during separation. The DPE value of H<sub>3</sub>PW<sub>12</sub>O<sub>40</sub> is significantly smaller (1087 kJ mol<sup>-1</sup> [19,20]) than the narrow range for different zeolite frameworks (1170–1200 kJ mol<sup>-1</sup> for CHA, BEA, FAU, MFI, and MOR [14,18,20–22]). In Section 3.2, we compare homologation rates and selectivities on BEA to those on zeolites with different pore sizes (FAU and MFI) and on SiO<sub>2</sub>–Al<sub>2</sub>O<sub>3</sub>, the mesoporous analog of aluminosilicate zeolites, to probe the consequences of spatial constraints on the relative rates of methylation, hydride transfer, and isomerization reactions during DME homologation.

### 3.1. Effects of acid strength on rates and selectivities of products from C<sub>1</sub> homologation

#### 3.1.1. Effects of acid strength in the presence and absence of spatial constraints

DME homologation turnover rates (Table 1a) were significantly higher on H<sub>3</sub>PW<sub>12</sub>O<sub>40</sub>/SiO<sub>2</sub> ( $7.3 \times 10^{-3}$  mol C [mol H<sup>+</sup> s]<sup>-1</sup>) than on SiO<sub>2</sub>–Al<sub>2</sub>O<sub>3</sub> ( $0.37 \times 10^{-3}$  mol C [mol H<sup>+</sup> s]<sup>-1</sup>), indicating that acid strength strongly influences DME homologation rates. The effect of acid strength on rates reflects electrostatic interactions between anionic conjugate bases and cations during deprotonation (i.e., a proton) and at late ion-pair transition states (i.e., protonated reactants) prevalent in acid-catalyzed reactions, as shown for alkanol elimination and alkoxide isomerization reactions [14,19,20,22,23]. Protonation of reactants at transition states of kinetically-relevant

**Table 1**

Rates and hydrocarbon isomer selectivities for dimethyl ether homologation on solid acids of varying (a) acid strength and (b) confinement at 473 K. Reactions were carried out at total carbon conversions less than 5%. The suffix -tyl refers to both alkane and alkene species of a given isomer structure.

(a) Catalyst	BEA	H <sub>3</sub> PW <sub>12</sub> O <sub>40</sub> /SiO <sub>2</sub>	SiO <sub>2</sub> -Al <sub>2</sub> O <sub>3</sub>	Equilibrium value <sup>c</sup>
Deprotonation energy (kJ mol <sup>-1</sup> )	1185 <sup>a</sup>	1087 <sup>a</sup>	–	
Rate (10 <sup>-3</sup> mol C [mol H <sup>+</sup> s] <sup>-1</sup> ) <sup>b</sup>	1.5	7.3	0.37	
Isomer selectivity within C <sub>n</sub> (%)				
Isobutyl	82	54	78	57
Isopentyl	97	91	95	68
2,3-Dimethylbutyl	47	43	51	12
Isohexyl	51	49	45	42
Triptyl	76	41	56	2.5
Dimethylpentyl + isoheptyl	24	59	44	89
(b) Catalyst	BEA	FAU	MFI	Equilibrium value <sup>c</sup>
Rate (10 <sup>-3</sup> mol C [mol H <sup>+</sup> s] <sup>-1</sup> ) <sup>b</sup>	1.5	3.3	2.1	
Isomer selectivity within C <sub>n</sub> (%)				
Isobutyl	82	86	60	57
Isopentyl	97	98	95	68
2,3-Dimethylbutyl	47	59	32	12
Isohexyl	51	40	65	42
Triptyl	76	81	11	2.5
Dimethylpentyl + isoheptyl	24	17	88	89

<sup>a</sup> See Refs. [14,18–20].

<sup>b</sup> Total rate of C consumed normalized by accessible H<sup>+</sup> determined from titration with 2,6-di-*tert*-butylpyridine as described in Section 2.1 and Ref. [13].

<sup>c</sup> Determined from D.R. Stull, E.F. Westrum, G.C. Sinke, The Chemical Thermodynamics of Organic Compounds, John Wiley and Sons, New York, 1969.

steps and the formation of the conjugate anion become more endothermic as acids weaken because they require charge separation. As a result, ion-pairs at transition states become more stable and activation barriers decrease on stronger acids (i.e., lower DPE). The effects of acid strength are rigorously discussed in Section 3.1.2 using thermochemical descriptions of the activation barriers that determine homologation rates and selectivities.

H<sub>3</sub>PW<sub>12</sub>O<sub>40</sub>/SiO<sub>2</sub> gave higher selectivities to C<sub>4</sub> hydrocarbons (40% vs. 35%; Fig. 1a) and lower combined selectivities to C<sub>5</sub>–C<sub>7</sub> hydrocarbons (38% vs. 54%; Fig. 1a) than SiO<sub>2</sub>-Al<sub>2</sub>O<sub>3</sub>. Ratios of isobutyl to *n*-butyl species within C<sub>4</sub> products were lower on H<sub>3</sub>PW<sub>12</sub>O<sub>40</sub>/SiO<sub>2</sub> than SiO<sub>2</sub>-Al<sub>2</sub>O<sub>3</sub> (1.2 vs. 3.5, Fig. 2a). Previous studies of DME homologation chain growth pathways on BEA showed that linear C<sub>4</sub> species have lower termination probabilities (defined in Section 2.2) than isobutyl species [7]. Therefore, *n*-butyl species preferentially grow to larger hydrocarbons [5–7] and isobutyl species terminate as isobutane on BEA. Higher selectivities to C<sub>4</sub> products, and specifically to linear butyl species, on H<sub>3</sub>PW<sub>12</sub>O<sub>40</sub>/SiO<sub>2</sub> (Fig. 2a) reflect higher termination probabilities for *n*-butyl species on H<sub>3</sub>PW<sub>12</sub>O<sub>40</sub>/SiO<sub>2</sub> than on SiO<sub>2</sub>-Al<sub>2</sub>O<sub>3</sub> and indicate that rates of hydride transfer increase relative to methylation rates as acid sites become stronger.

Selectivities to isomers with the four-carbon backbone of triptane within C<sub>5</sub>–C<sub>7</sub> products are lower on H<sub>3</sub>PW<sub>12</sub>O<sub>40</sub>/SiO<sub>2</sub> than on SiO<sub>2</sub>-Al<sub>2</sub>O<sub>3</sub> (Fig. 2b–d). Specifically, the ratios of isopentyl to *n*-pentyl (10 vs. 19), 2,3-dimethylbutyl to isohexyl (0.9 vs. 1.1), and triptyl to non-triptyl isomers (0.7 vs. 1.3) were smaller on H<sub>3</sub>PW<sub>12</sub>O<sub>40</sub>/SiO<sub>2</sub> than on SiO<sub>2</sub>-Al<sub>2</sub>O<sub>3</sub>. Previous studies of the mechanism of DME homologation on BEA showed that low isomerization rates of molecules with a four-carbon backbone relative to their hydride transfer and methylation rates prevent deviations from the preferred methylation path that selectively forms triptane [7]. Isomerized alkanes (i.e., those without the backbone of triptane) appear only as minor products on BEA, because rapid methylation steps grow isomerized alkenes to C<sub>8</sub>+ species that then undergo facile β-scission to form isobutane [5–7]. Therefore, high selectivities to isomers that are not formed along the methylation path to triptane on H<sub>3</sub>PW<sub>12</sub>O<sub>40</sub>/SiO<sub>2</sub> reflect higher rates of alkoxide isomerization and their preferential termination as alkanes before subsequent methylation reactions grow them to chains that can

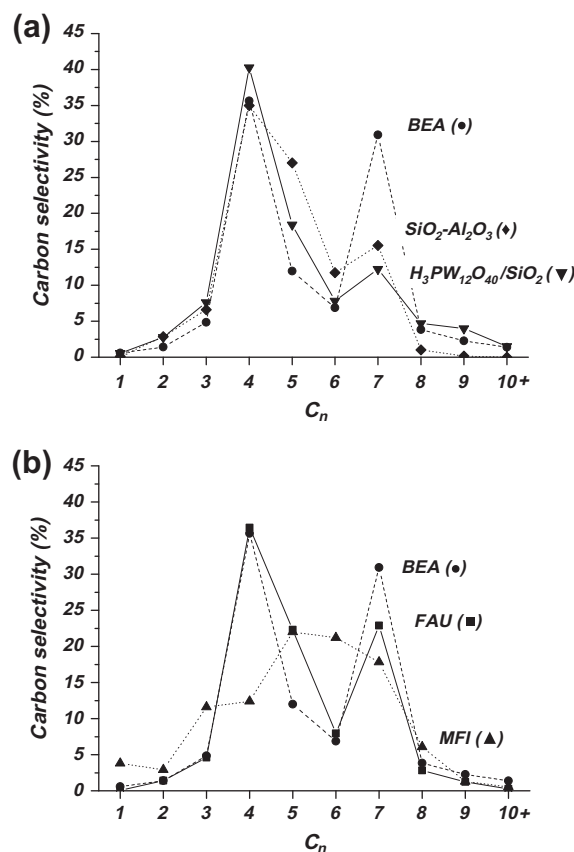


**Fig. 1.** Product selectivities (carbon basis) for reactions of DME (70–85 kPa) and propene (1.8–3.2 kPa) on (a) BEA (●), 5 wt.% H<sub>3</sub>PW<sub>12</sub>O<sub>40</sub>/SiO<sub>2</sub> (▼), and SiO<sub>2</sub>-Al<sub>2</sub>O<sub>3</sub> (◆) and (b) BEA (●), FAU (■), and MFI (▲) at 473 K. All reactions were carried out at less than 5% conversion (carbon basis) and 101 kPa total pressure (Ar balance).

undergo β-scission to form isobutyl species. Selectivities to isobutane within C<sub>4</sub> products are lower on H<sub>3</sub>PW<sub>12</sub>O<sub>40</sub>/SiO<sub>2</sub> than SiO<sub>2</sub>-Al<sub>2</sub>O<sub>3</sub> as a result of these higher rates of hydride transfer, which

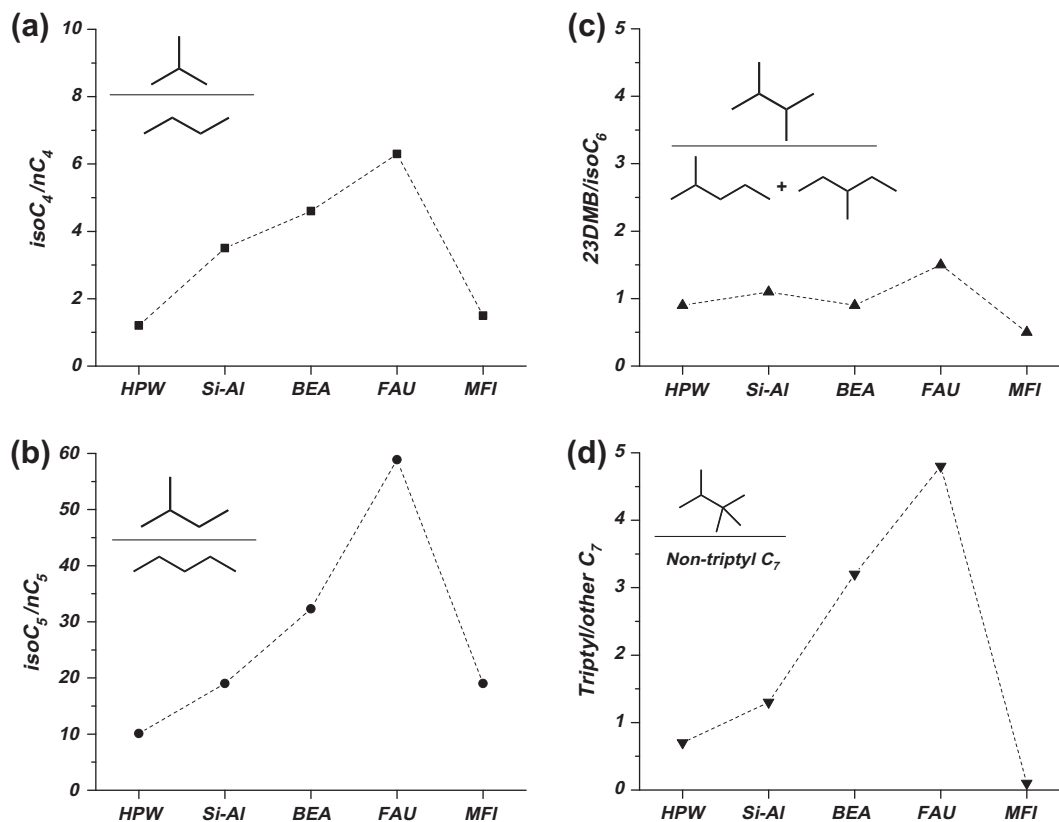


**Fig. 2.** (a) Isobutyl-to-*n*-butyl, (b) isopentyl-to-*n*-pentyl, (c) 2,3-dimethylbutyl-to-iso-hexyl, and (d) triptyl-to-non-triptyl isomer ratios for reactions of DME (70–85 kPa) and propene (1.8–3.2 kPa) on BEA, FAU, MFI, 5 wt.% H<sub>3</sub>PW<sub>12</sub>O<sub>40</sub>/SiO<sub>2</sub> (HPW), and SiO<sub>2</sub>-Al<sub>2</sub>O<sub>3</sub> (Si-Al) at 473 K. All reactions were carried out at less than 5% conversion (carbon basis) and 101 kPa total pressure (Ar balance). The “-tyl” suffix refers to all alkene and alkane species with a given backbone structure.

terminate isomerized products before they can undergo  $\beta$ -scission. We conclude that stronger acid sites preferentially increase isomerization and hydride transfer rates over methylation rates and lead to higher selectivities to C<sub>5</sub>–C<sub>7</sub> isomers without the four-carbon backbone of triptane as well as lower isobutane selectivities within C<sub>4</sub> products on H<sub>3</sub>PW<sub>12</sub>O<sub>40</sub>/SiO<sub>2</sub> compared to SiO<sub>2</sub>-Al<sub>2</sub>O<sub>3</sub>.

DME homologation turnover rates (Table 1a) are higher on H<sub>3</sub>PW<sub>12</sub>O<sub>40</sub>/SiO<sub>2</sub> ( $7.3 \times 10^{-3}$  mol C [mol H<sup>+</sup> s]<sup>-1</sup>) than BEA ( $1.5 \times 10^{-3}$  mol C [mol H<sup>+</sup> s]<sup>-1</sup>), and both of these acids have significantly higher rates than SiO<sub>2</sub>-Al<sub>2</sub>O<sub>3</sub> ( $0.37 \times 10^{-3}$  mol C [mol H<sup>+</sup> s]<sup>-1</sup>). These results indicate that stronger acids and sites confined within zeolite pores lead to higher DME homologation rates, but that the greater acid strength of H<sub>3</sub>PW<sub>12</sub>O<sub>40</sub>/SiO<sub>2</sub> affects rates more strongly than the confinement provided by BEA channels. The effects of confinement depend on the relative stabilization of transition states and adsorbed intermediates by the stronger van der Waals interactions prevalent within zeolite channels. The effects of confinement on measured barriers and turnover rates depend on whether the relevant barriers reflect transition-state energies relative to extra-zeolite or intra-zeolite reactants, as we discuss in detail in Section 3.2.

DME homologation selectivities to C<sub>4</sub> hydrocarbons (Fig. 1a) are slightly higher on H<sub>3</sub>PW<sub>12</sub>O<sub>40</sub>/SiO<sub>2</sub> (41%) than BEA (36%). Ratios of isobutyl to *n*-butyl isomers within C<sub>4</sub> species (Table 1a and Fig. 2a) are lower on H<sub>3</sub>PW<sub>12</sub>O<sub>40</sub>/SiO<sub>2</sub> (1.2) than BEA (4.6). The higher selectivity to C<sub>4</sub> species, and specifically to *n*-butyl isomers, on H<sub>3</sub>PW<sub>12</sub>O<sub>40</sub>/SiO<sub>2</sub> relative to BEA, reflects the preferential enhancement of hydride transfer rates over methylation with increasing acid strength, which increases the probability of termination of *n*-butyl species as *n*-butane and, in turn, decreases isobutyl-to-*n*-butyl isomer ratios. These higher

hydride transfer rates on H<sub>3</sub>PW<sub>12</sub>O<sub>40</sub>/SiO<sub>2</sub> also decrease isobutyl selectivities by terminating isomerized species before subsequent methylation to C<sub>8+</sub> and  $\beta$ -scission reactions of these latter species.

Similar to SiO<sub>2</sub>-Al<sub>2</sub>O<sub>3</sub>, BEA shows higher selectivities to C<sub>5</sub>–C<sub>7</sub> hydrocarbons (50% vs. 38%; Fig. 1a) and to triptyl isomers (triptyl-to-non-triptyl ratios of 3.2 and 0.7; Fig. 2d) than H<sub>3</sub>PW<sub>12</sub>O<sub>40</sub>/SiO<sub>2</sub>. The higher selectivities to isomers without the four-carbon backbone of triptane on H<sub>3</sub>PW<sub>12</sub>O<sub>40</sub>/SiO<sub>2</sub> relative to BEA indicate that stronger acids also favor isomerization over methylation rates. As a result, alkenes rearrange their backbone more frequently before methylation to triptane on H<sub>3</sub>PW<sub>12</sub>O<sub>40</sub>/SiO<sub>2</sub>; the preferential increase in hydride transfer rates by strong acids leads to the termination of these isomerized chains before they methylate to C<sub>8+</sub> chains and form isobutane by  $\beta$ -scission. The lower triptane selectivities on H<sub>3</sub>PW<sub>12</sub>O<sub>40</sub>/SiO<sub>2</sub> compared with BEA confirm that increasing acid strength increases isomerization and hydride transfer rates more than methylation rates and extends these conclusions to comparisons between strong acid sites on H<sub>3</sub>PW<sub>12</sub>O<sub>40</sub>/SiO<sub>2</sub> and aluminosilicates with weaker acid sites in confined (BEA) and unconfined (SiO<sub>2</sub>-Al<sub>2</sub>O<sub>3</sub>) locations.

Next, we use reactions between <sup>13</sup>C-DME and <sup>12</sup>C-2,3-dimethyl-2-butene to measure individual rates of methylation, hydride transfer, and isomerization and to determine termination ( $\beta$ ), skeletal isomerization ( $\gamma_{sk}$ ), and  $\beta$ -scission ( $\gamma_{\beta s}$ ) probabilities for 2,3-dimethylbutyl species (Fig. 3). These data also address the effects of acid strength on interactions between carbenium ions and the conjugate bases that stabilize transition states for methylation, hydride transfer, and isomerization reactions to different extents, which, in turn, cause these reactions to “sense” acid strength differently.

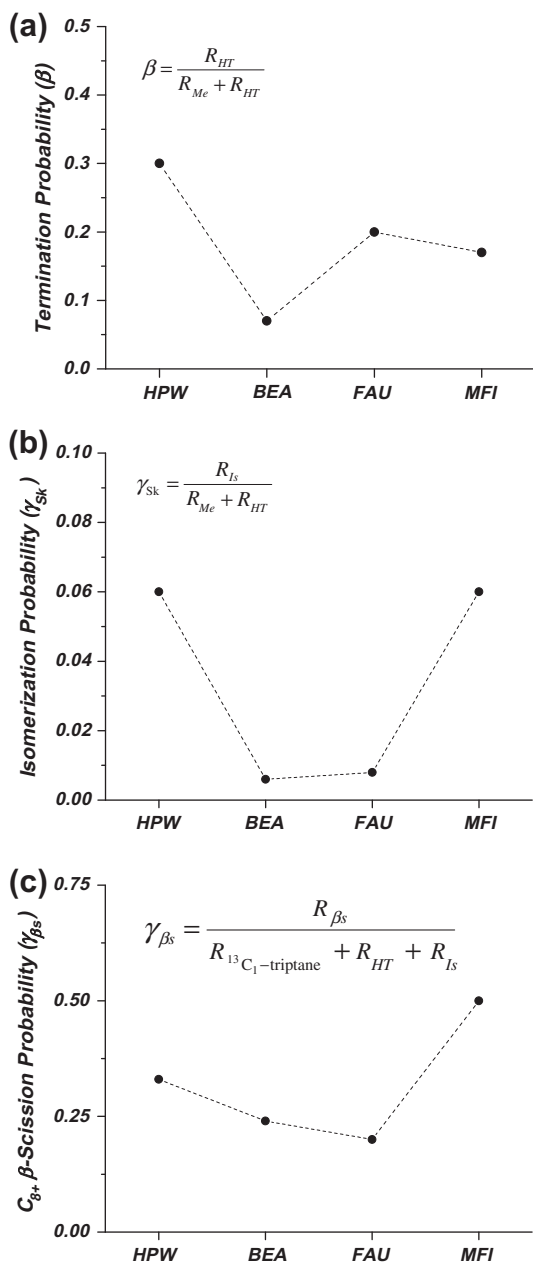


**Fig. 3.** (a) Termination ( $\beta$ ), (b) isomerization ( $\gamma_{sk}$ ), and (c)  $C_{8+}$   $\beta$ -scission ( $\gamma_{\beta s}$ ) probabilities from co-reactions of  $^{13}\text{C}$ -dimethyl ether (87 kPa) and  $^{12}\text{C}$ -2,3-dimethyl-2-butene (0.6 kPa) on 5 wt.%  $\text{H}_3\text{PW}_{12}\text{O}_{40}/\text{SiO}_2$  (HPW), BEA, MFI, and FAU at 473 K. Reactions carried out at less than 2% total carbon conversion and 101 kPa total pressure (He balance). Probabilities were calculated as described in Section 2.1, Supporting information, and Ref. [7].  $R_{HT}$ ,  $R_{Me}$ , and  $R_{Is}$  refer to rates of hydride transfer, methylation, and isomerization (determined as in Ref. [7] and Supporting information).

### 3.1.2. Effects of acid strength on selectivities among methylation, hydride transfer, and isomerization reactions

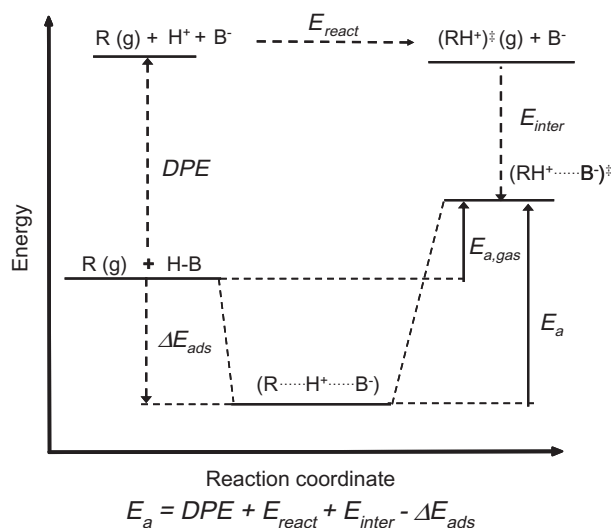
Termination ( $\beta$ ) and isomerization ( $\gamma_{sk}$ ) probabilities of 2,3-dimethylbutyl species (Fig. 3a and b), measured from isotopic  $^{13}\text{C}$ -DME homologation reactions, are larger on  $\text{H}_3\text{PW}_{12}\text{O}_{40}/\text{SiO}_2$  (0.30 and 0.06, respectively) than on BEA (0.07 and 0.006, respectively). The values of these probabilities are consistent with the higher selectivities to  $C_4$  products, *n*-butane within  $C_4$  products, and non-triptane isomers observed on  $\text{H}_3\text{PW}_{12}\text{O}_{40}/\text{SiO}_2$  compared with BEA or  $\text{SiO}_2\text{-Al}_2\text{O}_3$  (Section 3.1.1).  $C_{8+}$   $\beta$ -scission probabilities ( $\gamma_{\beta s}$ ; defined by Eq. (2) in Section 2.2) are slightly larger on

$\text{H}_3\text{PW}_{12}\text{O}_{40}/\text{SiO}_2$  (0.33; Fig. 3c) than on H-BEA (0.24), indicating that more chains originating from  $^{12}\text{C}$ -2,3-dimethylbutene form  $C_{8+}$  and undergo subsequent  $\beta$ -scission on  $\text{H}_3\text{PW}_{12}\text{O}_{40}/\text{SiO}_2$  than on BEA. The larger  $\gamma_{\beta s}$  values on  $\text{H}_3\text{PW}_{12}\text{O}_{40}/\text{SiO}_2$  compared with BEA reflect higher concentrations of isomerized products, which methylate to  $C_{8+}$  chains that undergo  $\beta$ -scission more readily than triptyl precursors. We conclude from these data that stronger acid sites increase hydride transfer and isomerization rates for alkoxides more than methylation rates of the respective alkenes formed via desorption of these alkoxides.

The effects of acid strength on reaction rates were previously examined for alkanol dehydration, ether cleavage, and alkene isomerization on Keggin polyoxometalate clusters and zeolite BEA in its acid form [22–24]. The strengths of Brønsted acid sites on these catalysts were assessed from their deprotonation energies (DPE), which are available from *ab initio* calculations because of their known inorganic structures [18,19]. Rate constants measured on these solid acids decreased exponentially with increasing DPE, indicating the predominant role of DPE in determining activation barriers. The effects of DPE on activation barriers were illustrated using Born–Haber thermochemical cycles that exploit the path-independent properties of state functions to dissect activation barriers into specific properties of reactants and catalysts accessible to experiment or theory (Scheme 2). Acid-catalyzed transformations of adsorbed intermediates involving late ion-pair transition states exhibit activation barriers ( $E_a$ ) with contributions from (i) deprotonation of the acid (DPE), (ii) adsorption of reactants ( $\Delta E_{ads}$ ), (iii) gas-phase reactions between protons and reactants to form the gaseous analogs of the organic cations at transition states ( $E_{react}$ ), and (iv) interactions between these gaseous cations and the conjugate anion formed via deprotonation of the solid acid ( $E_{inter}$ ):

$$E_a = \text{DPE} + E_{react} + E_{inter} - \Delta E_{ads} \quad (3)$$

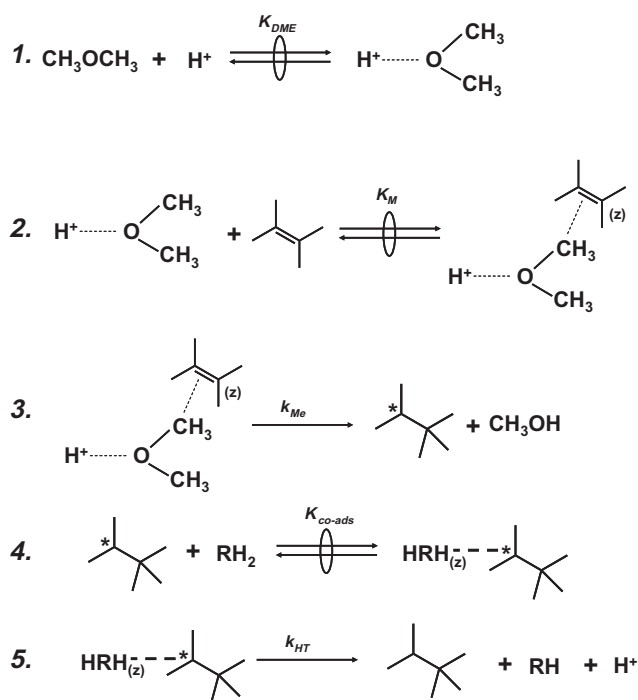
The DPE and  $E_{react}$  terms only depend on properties of catalysts and reactant molecules, respectively, while  $E_{inter}$  and  $\Delta E_{ads}$  reflect how molecules and catalysts interact. Adsorption energies ( $\Delta E_{ads}$ ) depend on specific interactions between reactants and active sites and may include contributions from hydrogen bonding, electrostatic interactions in ion-pairs, and covalent bonds between



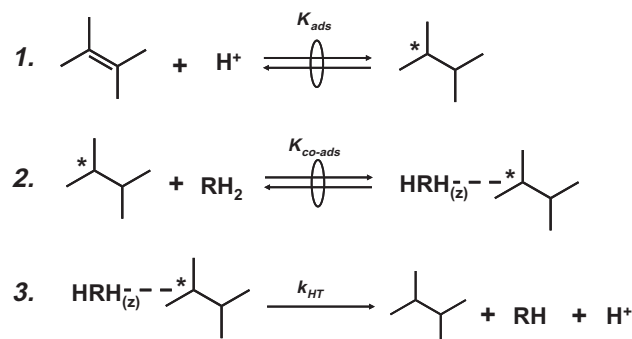
**Scheme 2.** Thermochemical cycle for activation barriers ( $E_a$ ) of acid-catalyzed reactions. Activation barriers depend on the acid's (HB) deprotonation energy (DPE), protonation energies ( $E_{react}$ ) of gas-phase reactants (R), interaction energies between protonated transition states and the conjugate anion ( $E_{inter}$ ), and reactant adsorption energies ( $\Delta E_{ads}$ ). Activation barriers measured with respect to gas-phase reactants ( $E_{a,gas}$ ) do not have contributions from adsorption energies. The double dagger indicates the ion pair transition states.

reactants and binding sites. van der Waals interactions also influence adsorption energies, especially within confined spaces [25–27]. Organic moieties at transition states can interact with catalysts via the same interactions as adsorbed reactants, but electrostatic interactions contribute to the predominant stabilization at the late ion-pair transition states ubiquitous in Brønsted acid catalysis. The barriers responsible for measured rates reflect energy differences between the transition state for the kinetically-relevant step and the intermediate that forms it when active sites are saturated with such intermediates during steady-state catalysis, and in such cases, the measured barriers include contributions from all terms in Eq. (3). When sites are predominantly uncovered, measured barriers and rates reflect energy differences between transition states for the kinetically-relevant step and the gas-phase reactants; these barriers do not depend on adsorption energies (i.e.,  $\Delta E_{\text{ads}}$  is not a component of Eq. (3); depicted in Scheme 2 as  $E_{\text{a,gas}}$ ). These two situations represent extremes in active site occupation and can be used to assess the relevance of reactant adsorption in determining rates and activation barriers for methylation, hydride transfer, and isomerization reactions that occur during  $C_1$  homologation.

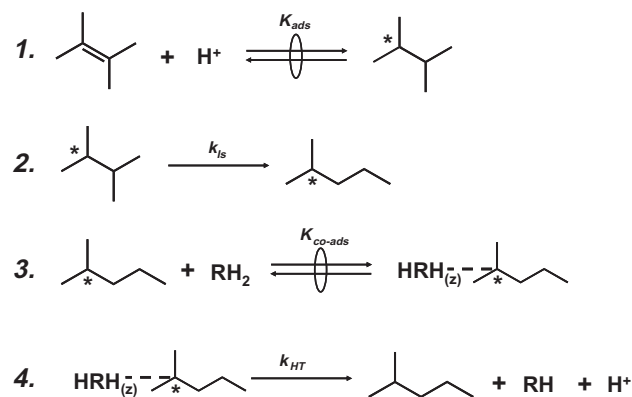
Next, we consider the effects of acid strength on the relative rates of hydride transfer, isomerization, and methylation reactions by using rate equations derived from their respective elementary steps (depicted in Schemes 3–5 with 2,3-dimethyl-2-butene as a prototypical alkene; all equations derived in the Supporting information). Methylation steps (Scheme 3) involve adsorption of DME at protons (Step 1) and their subsequent reactions with vicinal alkenes adsorbed within zeolite channels (Step 2) [28] mediated by late transition states. DME is fully protonated at this transition state and one of its methyl groups is transferred to the alkene as the C–O bond cleaves and the new C–C bond forms (Step 3). The



**Scheme 3.** Elementary steps for alkene (shown as 2,3-dimethyl-2-butene) methylation by dimethyl ether (DME). Asterisks (\*) indicate preferred attachment locations of alkoxides to the surface. Subscript "(z)" indicates species adsorbed within zeolite channels near Brønsted sites.  $K_{\text{DME}}$  and  $K_{\text{M}}$  are adsorption equilibrium constants for DME at protons and co-adsorption of the alkene, respectively, and  $k_{\text{Me}}$  is the methylation rate constant.  $K_{\text{co-ads}}$  is the adsorption equilibrium constant for hydride donors ( $\text{RH}_2$ ) near methylated alkoxides and  $k_{\text{HT}}$  is the hydride transfer rate constant.



**Scheme 4.** Elementary steps for hydride transfer from donor molecules ( $\text{RH}_2$ ) to alkenes (shown as 2,3-dimethyl-2-butene). Asterisks indicate preferred attachment locations of alkoxides to the surface. Subscript "(z)" indicates species adsorbed within zeolite channels near Brønsted sites.  $K_{\text{ads}}$  and  $K_{\text{co-ads}}$  are adsorption equilibrium constants for alkene adsorption at protons and co-adsorption of the hydride donor, respectively, and  $k_{\text{HT}}$  is the hydride transfer rate constant.



**Scheme 5.** Elementary steps for alkene isomerization (shown as 2,3-dimethyl-2-butene). Asterisks indicate the preferred attachment location of alkoxides to the surface. Subscript "(z)" indicates species adsorbed within zeolite channels near Brønsted sites.  $K_{\text{ads}}$  and  $K_{\text{co-ads}}$  are adsorption equilibrium constants for adsorption of the alkene at protons and co-adsorption of the hydride donor ( $\text{RH}_2$ ) near isomerized alkenes, respectively.  $k_{\text{is}}$  and  $k_{\text{HT}}$  are the isomerization and hydride transfer rate constants, respectively.

products desorb as either an alkene (via alkoxide deprotonation) or an alkane (via hydride transfer) (Steps 4 and 5). Scheme 4 shows elementary hydride transfer reactions between gaseous hydride donors ( $\text{RH}_2$ ) and alkene acceptors (R'H). Protonation of alkenes forms alkoxides (Step 1), which react with vicinal hydride donors solvated within channels (Step 2) via carbenium ion transition states to form alkanes ( $\text{R}'\text{H}_2$ ) and alkenes (RH) and re-form protons (Step 3) [9]. Alkene isomerization (Scheme 5) occurs via the formation of alkoxides (Step 1) that react via monomolecular cyclopropyl carbenium ion transition states [29] to form alkoxide isomers (Step 2). These isomers desorb as alkenes via deprotonation or as alkanes via hydride transfer (Steps 3 and 4).

Rate equations for methylation, hydride transfer, and isomerization were derived (Supporting information) by assuming pseudo-steady-state concentrations of all surface intermediates and quasi-equilibrated alkene and DME interactions with protons (Step 1, Schemes 3–5) and quasi-equilibrated alkene (Step 2 in Scheme 3) and alkane (Step 4 in Scheme 3, Step 2 in Scheme 4, and Step 3 in Scheme 5) adsorption within zeolite channels near active sites. The denominators in these rate expressions reflect the occupation of sites by various adsorbed intermediates and are identical for all reactions occurring at Brønsted acid sites. As a result, rate ratios are independent of these occupations (Supporting information).

The ratios of hydride transfer or isomerization rates ( $r_{HT}$  and  $r_{Is}$ , respectively) to methylation rates ( $r_{Me}$ ) are then:

$$\frac{r_{HT}}{r_{Me}} = \frac{k_{HT}K_{ads}K_{co-ads}(RH_2)}{k_{Me}K_{DME}K_M(DME)} \quad (4)$$

$$\frac{r_{Is}}{r_{Me}} = \frac{k_{Is}K_{ads}}{k_{Me}K_{DME}K_M(DME)} \quad (5)$$

in which rate and equilibrium constants refer to the elementary steps in Schemes 3–5. Scheme 6 shows individual rate and equilibrium constants in these pathways in terms of free energy changes for elementary reactions. Products of equilibrium and rate constants appearing in Eqs. (4) and (5) are effective rate constants ( $k_{eff}$  in Scheme 6) and reflect only the difference in free energy between transition states of the kinetically-relevant steps of methylation (Scheme 3, Step 3), hydride transfer (Scheme 4, Step 3), and isomerization (Scheme 5, Step 2) reactions and their respective gas-phase reactants. Adsorbed intermediates influence rates through their contributions to site balances; however, these dependences are absent here because site balances cancel in ratios of rates. As a result, identities of adsorbed intermediates that precede the transition states are kinetically irrelevant for ratios of rates and their free energies do not contribute to values of effective rate constants.

The effects of acid strength on the relative rates of hydride transfer, isomerization, and methylation (Section 3.1.1) and their corresponding effective rate constants are examined next using thermochemical cycles to describe their respective activation barriers measured with respect to gas-phase reactants ( $E_{a,gas}$  in Scheme 2). The difference between activation barriers of hydride transfer and methylation reactions on a given catalyst, which is consequential for the ratio of their rates (Eq. (4)), is only influenced by their transition-state interaction energies ( $E_{inter}$ ) and gas-phase reactant protonation energies ( $E_{react}$ ) according to the relation:

$$E_{a,gas}^{HT} - E_{a,gas}^{Me} = (E_{inter}^{HT} - E_{inter}^{Me}) + (E_{react}^{HT} - E_{react}^{Me}) \quad (6a)$$

in which the superscripts “HT” and “Me” denote the energy terms in the hydride transfer and methylation thermochemical cycles (Scheme S2 in the Supporting information). Similarly, the relative rates of isomerization (denoted by the “Is” superscript) and methylation reactions are determined by differences in their  $E_{inter}$  and  $E_{react}$  values:

$$E_{a,gas}^{Is} - E_{a,gas}^{Me} = (E_{inter}^{Is} - E_{inter}^{Me}) + (E_{react}^{Is} - E_{react}^{Me}) \quad (6b)$$

The effects of acid strength on the relative activation barriers of hydride transfer, isomerization, and methylation reactions are then determined by the derivative of Eqs. (6a) and (6b) with respect to DPE:

$$\frac{d(E_{a,gas}^{HT} - E_{a,gas}^{Me})}{d(DPE)} = \frac{d(E_{inter}^{HT})}{d(DPE)} - \frac{d(E_{inter}^{Me})}{d(DPE)} \quad (7a)$$

$$\frac{d(E_{a,gas}^{Is} - E_{a,gas}^{Me})}{d(DPE)} = \frac{d(E_{inter}^{Is})}{d(DPE)} - \frac{d(E_{inter}^{Me})}{d(DPE)} \quad (7b)$$

The protonation energies of reactants do not appear in Eqs. (7a) and (7b), because they reflect properties of gas-phase reactions, which do not depend on catalyst properties ( $d(E_{react})/d(DPE) = 0$ ). Therefore, acid strength influences differences in activation barriers only through dependences of transition-state interaction energies on DPE (Eq. 7). Next, we examine the charge distributions of cations at methylation, isomerization, and hydride transfer transition states, which determine the dependences of their interaction energies on acid strength.

Transition states calculated by density functional theory consist of ion-pairs in methylation of alkenes with methanol [30], hydride transfer from alkanes to alkoxides [9,31], and isomerization of alkoxides [29,32], consistent with the ubiquitous role of full ion-pairs at transition states for reactions catalyzed by Brønsted acids. Methyl groups in alkene methylation transition states have fully

Methylation	Hydride Transfer	Isomerization
$r_{Me} = \frac{k_{Me}K_MK_{DME}(DME)(R'H)}{(\theta)}$	$r_{HT} = \frac{k_{HT}K_{ads}K_{co-ads}(R'H)(RH_2)}{(\theta)}$	$r_{Is} = \frac{k_{Is}K_{ads}(R'H)}{(\theta)}$
$K_{DME} = \exp(-\Delta G_{DME})$ $DME + H^+ \rightleftharpoons DME^*$	$K_{ads} = \exp(-\Delta G_{ads})$ $R'H + H^+ \rightleftharpoons R'H^*$	$K_{ads} = \exp(-\Delta G_{ads})$ $R'H + H^+ \rightleftharpoons R'H^*$
$K_M = \exp(-\Delta G_M)$ $DME^* + R'H \rightleftharpoons R'H-DME^*$	$K_{co-ads} = \exp(-\Delta G_{co-ads})$ $R'H^* + RH_2 \rightleftharpoons RH_2-R'H^*$	
$k_{Me} = \exp(-\Delta G_{a,Me})$ $R'H-DME^* \longrightarrow TS_{Me}$	$k_{HT} = \exp(-\Delta G_{a,HT})$ $RH_2-R'H^* \longrightarrow TS_{HT}$	$k_{Is} = \exp(-\Delta G_{a,Is})$ $R'H^* \longrightarrow TS_{Is}$
$k_{eff} = k_{Me}K_MK_{DME}$ $= \exp(-\Delta G_{DME} - \Delta G_M - \Delta G_{a,Me})$ $R'H + DME + H^+ \longrightarrow TS_{Me}$	$k_{eff} = k_{HT}K_{ads}K_{co-ads}$ $= \exp(-\Delta G_{ads} - \Delta G_{co-ads} - \Delta G_{a,HT})$ $R'H + RH_2 + H^+ \longrightarrow TS_{HT}$	$k_{eff} = k_{Is}K_{ads}$ $= \exp(-\Delta G_{ads} - \Delta G_{a,Is})$ $R'H + H^+ \longrightarrow TS_{Is}$

**Scheme 6.** Rate expressions and their associated equilibrium and rate constants in terms of free energy changes for alkene methylation (R'H) by dimethyl ether (DME), hydride transfer between alkenes and hydride donors (RH<sub>2</sub>), and alkene isomerization. Denominators of rate expressions ( $\theta$ ) reflect occupancies of active sites by intermediates and are the same for all reactions (Supporting information). Free energy changes refer to the reaction illustrated below the rate or equilibrium constant. Structures of the intermediates are shown in the corresponding elementary reactions in Schemes 3–5. “TS” denotes a transition state.

transferred to the less-substituted carbon atom at the alkene double bonds [30], leaving the charge localized at the other carbon atom in the double bond. In contrast, cyclopropyl transition states involved in alkoxide isomerization have the positive charge delocalized among all carbons [29,32], making it more diffuse than at methylation transition states. At the hydride transfer transition state, the alkoxide C–O bond is cleaved and the carbenium ion formed abstracts a hydride from the donor [9]. This hydride is shared between the donor and acceptor, but remains closer to the less-substituted carbon atom in the complex. In hydride transfer from propane to a propoxide, the C–H bond in propane is elongated at the transition state; taken together with Mulliken charges, this indicates that the charge is effectively delocalized between the donor and the acceptor molecules. The charges are more diffuse in hydride transfer and isomerization transition states than in methylation transition states; as a result, methylation transition states interact more strongly with the conjugate anion. More highly charged conjugate anions are less stable and lead to higher DPE values [23], as well as to more negative transition-state interaction energies ( $E_{\text{inter}}$ ) because their ion-pairs have stronger electrostatic forces ( $d(E_{\text{inter}})/d(\text{DPE}) < 0$ ). The effects of acid strength on interaction energies are stronger for methylation transition states than hydride transfer and isomerization transition states ( $\frac{d(E_{\text{inter}}^{\text{Me}})}{d(\text{DPE})} < \frac{d(E_{\text{inter}}^{\text{HT}})}{d(\text{DPE})} < 0$  in Eq. (7a) and  $\frac{d(E_{\text{inter}}^{\text{Me}})}{d(\text{DPE})} < \frac{d(E_{\text{inter}}^{\text{Is}})}{d(\text{DPE})} < 0$  in Eq. (7b)) because cations at methylation transition states have localized charges that are more similar to a proton. Such organic cations more effectively recover the energy required to protonate reactants, which is reflected in DPE values, causing methylation activation barriers to be less sensitive to DPE than for isomerization or hydride transfer ( $\frac{d(E_{\text{a, gas}}^{\text{HT}} - E_{\text{a, gas}}^{\text{Me}})}{d(\text{DPE})} > 0$  in Eq. (7a) and  $\frac{d(E_{\text{a, gas}}^{\text{Is}} - E_{\text{a, gas}}^{\text{Me}})}{d(\text{DPE})} > 0$  in Eq. (7b)). Locally charged cations at alkanol dehydration transition states accounted for the weaker effects of DPE on elimination activation barriers compared to isomerization activation barriers in a previous study [22]. These conclusions are consistent with the higher termination and isomerization probabilities measured on  $\text{H}_3\text{PW}_{12}\text{O}_{40}/\text{SiO}_2$  (0.30 and 0.06, respectively) than on BEA (0.07 and 0.006, respectively), which also lead to lower selectivities to  $\text{C}_7$  hydrocarbons (12% vs. 31%) and triptyl isomers within  $\text{C}_7$  products (41% vs. 76%).

Strong acid sites on  $\text{H}_3\text{PW}_{12}\text{O}_{40}/\text{SiO}_2$  preferentially increase hydride transfer and isomerization rates more than methylation rates because cations with diffuse charges at their transition states recover less of the energy needed for deprotonation than localized cations at methylation transition states. As a result, stronger acid sites form triptane less selectively than weaker acid sites because hydrocarbons deviate from the preferred path more frequently and subsequently terminate on strong acids. Next, we probe the effects of solvation of transition states by spatial confinement by examining DME homologation rates and selectivities on  $\text{SiO}_2\text{-Al}_2\text{O}_3$  and on zeolites with diverse structures but similar acid strength (BEA, FAU, and MFI).

### 3.2. Effects of spatial constraints on rates and selectivities of products from $\text{C}_1$ homologation

#### 3.2.1. Effects of confinement within zeolite micropores on $\text{C}_1$ homologation chemistry

DME turnover rates are much smaller on  $\text{SiO}_2\text{-Al}_2\text{O}_3$  ( $0.37 \times 10^{-3} \text{ mol C} [\text{mol H}^+ \text{ s}]^{-1}$ ) than on BEA ( $1.5 \times 10^{-3} \text{ mol C} [\text{mol H}^+ \text{ s}]^{-1}$ ) and indicate that confinement within voids of molecular size increases DME homologation rates via preferential van der Waals stabilization of transition states relative to the relevant reacting intermediates for rates at these reaction conditions. Selectivities to isobutyl isomers within  $\text{C}_4$  hydrocarbons are also smaller

on  $\text{SiO}_2\text{-Al}_2\text{O}_3$  than on BEA (isobutyl-to-*n*-butyl ratios of 3.5 vs. 4.6; Fig. 2a). The lower isobutyl-to-*n*-butyl ratio measured on  $\text{SiO}_2\text{-Al}_2\text{O}_3$  indicates that confinement within channels of BEA increases methylation rates relative to hydride transfer steps, causing more *n*-butyl species to methylate to isopentyl species (as shown in previous studies [7]) rather than terminate as *n*-butane via hydride transfer. Also, the preference for methylation over termination derived from confinement leads to more  $\text{C}_{8+}$  hydrocarbons that undergo fast  $\beta$ -scission to isobutane and increase its selectivity on BEA.  $\text{C}_7$  selectivities (16% vs. 31%; Fig. 1b) and triptyl-to-non-triptyl isomer ratios in  $\text{C}_7$  chains (1.3 vs. 3.2; Table 1b, Fig. 2d) are smaller on  $\text{SiO}_2\text{-Al}_2\text{O}_3$  than BEA.  $\text{SiO}_2\text{-Al}_2\text{O}_3$  gave higher  $\text{C}_5$  selectivities (27% vs. 12%; Fig. 1b) and lower isopentyl-to-*n*-pentyl isomer (19 vs. 34; Fig. 2b) ratios than BEA. Lower selectivities to  $\text{C}_7$  products, triptane within  $\text{C}_7$  products, and *n*-pentyl isomers within  $\text{C}_5$  products on  $\text{SiO}_2\text{-Al}_2\text{O}_3$  compared to BEA indicate that confinement favors methylation steps that grow chains sequentially along the preferred path and hydride transfer steps that terminate these chains before significant isomerization.

Enhancement of homologation rates by solvation, with a preference for methylation and hydride transfer steps, is examined next using the thermochemical cycles introduced in Section 3.1.2 (Eq. (3) and Scheme 2). The confinement of acid sites within zeolite channels influences rates and selectivities because adsorbed intermediates and transition states are significantly stabilized by stronger van der Waals interactions with channel walls, which influence the values of  $\Delta E_{\text{ads}}$  and  $E_{\text{inter}}$  and their contributions to activation barriers in thermochemical cycles. When active sites are saturated with the immediate precursors to the kinetically-relevant transition states, activation barriers that are consequential for rates depend on the energy differences between transition states and these adsorbed precursors ( $E_{\text{a}}$  in Scheme 2). Activation barriers are insensitive to confinement under such conditions because additional van der Waals forces contribute similarly to  $\Delta E_{\text{ads}}$  and  $E_{\text{inter}}$  and their effects cancel each other in Eq. (3). For rates measured at conditions that maintain predominantly vacant sites, activation barriers that matter for rates reflect differences in energy between the transition-state and the gaseous reactants ( $E_{\text{a, gas}}$  in Scheme 2). In these instances,  $\Delta E_{\text{ads}}$  terms do not contribute to activation barriers and van der Waals forces decrease activation barriers by stabilizing transition states via  $E_{\text{int}}$ . Enhancement of reaction rates by selective van der Waals stabilization of transition states is evident in acid-catalyzed alkane cracking and dehydrogenation at conditions leading to predominantly vacant sites [25–27]; these van der Waals interactions stabilize transition states to a greater extent as the voids become similar in size to transition states [33–35]. Activation barriers for monomolecular cracking of *n*-alkanes ( $190\text{--}210 \text{ kJ mol}^{-1}$ ) on zeolites (FER, MFI, MOR, BEA, FAU) and amorphous  $\text{SiO}_2\text{-Al}_2\text{O}_3$  [26,27,36–43] are similar once alkane adsorption energies are corrected for and suggest that differences in rates are entirely caused by their respective abilities to solvate cracking transition states and not by different acid strengths. Thus, DPE values of aluminosilicate catalysts are not significantly influenced by confinement, and rates are higher on BEA than  $\text{SiO}_2\text{-Al}_2\text{O}_3$  only because enhanced stabilization of transition states with respect to gas-phase reactants decreases the relevant activation barriers on BEA compared to  $\text{SiO}_2\text{-Al}_2\text{O}_3$ .

The ratios of hydride transfer or isomerization rates to methylation rates (Eqs. (4) and (5)) and their respective effective rate constants ( $k_{\text{eff}}$  in Scheme 6) are influenced by van der Waals stabilization through the free energies of methylation, hydride transfer, and isomerization transition states. Selectivities of homologation products are influenced by the relative extents to which these transition states are stabilized by confinement. Confinement of acid sites within zeolite channels decrease activation barriers for methylation, hydride transfer, and isomerization reactions, because

van der Waals forces stabilize each of their transition states (via  $E_{\text{inter}}$  in Eq. (3)) without equivalent stabilization of their respective gas-phase reactants ( $E_{\text{a, gas}}$  in Scheme 2). Contributions to  $E_{\text{inter}}$  from van der Waals forces are larger for methylation and hydride transfer than for isomerization, however, because two gas-phase reactants are stabilized within zeolite pores at methylation and hydride transfer transition states, but only a single molecule at isomerization transition states. Thus, selectivities to  $C_7$  hydrocarbons and triptyl isomers within  $C_7$  products are higher on BEA (31% and 76%, respectively; Tables 1a and 1b) than  $\text{SiO}_2\text{-Al}_2\text{O}_3$  (16% selectivity to  $C_7$  and 56% triptyl isomers within  $C_7$  products; Table 1) because methylation and hydride transfer steps, whose transition states are preferentially stabilized by solvation over the isomerization analogs, preserve chains with a four-carbon backbone along the  $C_1$  homologation path. Next, we further probe the effects of confinement by comparing DME homologation rates and selectivities on large-pore (BEA and FAU) and medium-pore (MFI) zeolites that differ in the extent to which they stabilize methylation, hydride transfer, and isomerization transition states.

### 3.2.2. Effects of confinement within large pores on $C_1$ homologation chemistry

DME homologation turnover rates were larger on FAU than BEA ( $3.3 \times 10^{-3}$  vs.  $1.5 \times 10^{-3}$  mol C [mol  $\text{H}^+$  s] $^{-1}$ ). Both FAU and BEA preferentially formed  $C_4$  and  $C_7$  hydrocarbons (Fig. 1b). BEA gave slightly higher selectivities to  $C_7$  products than FAU (31% vs. 23%), but lower selectivities to  $C_5$  (12% vs. 23%) and  $C_6$  (6% vs. 8%) hydrocarbons (Fig. 1b). The predominant  $C_5$ ,  $C_6$ , and  $C_7$  isomers on BEA and FAU contained the backbone of triptane, but their ratios to isomers of the same carbon number (Fig. 2b–d) were higher on FAU than BEA (isopentyl-to- $n$ -pentyl = 59 vs. 32; 2,3-dimethylbutyl-to-isoheptyl = 1.5 vs. 0.9; triptyl-to-non-triptyl = 4.8 vs. 3.2). Higher selectivities to  $C_5$ – $C_6$  products with the four-carbon backbone of triptane on FAU suggest that chain termination probabilities are higher on FAU than BEA. Selectivities to  $C_4$  chains (36%) and to isobutyl isomers within  $C_4$  chains (82–86%) were similar on BEA and FAU. Binomial distributions of isobutane isotopologues from  $^{13}\text{C}$ -DME/ $^{12}\text{C}$ -alkene reactions [7] indicated the formation of isobutane via  $\beta$ -scission of  $C_{8+}$  chains and the formation of  $n$ -butyl species via propene methylation. Therefore, the selective formation of isobutyl over  $n$ -butyl species on FAU and BEA indicates that  $\beta$ -scission of  $C_{8+}$  chains is the preferential path for  $C_4$  formation on these catalysts.

$^{13}\text{C}$ -DME reactions with  $^{12}\text{C}$ -2,3-dimethyl-2-butene gave very low isomerization probabilities ( $\gamma_{\text{sk}}$ ) on BEA and FAU (0.006 and 0.008; Fig. 3), consistent with the prevalence of triptyl precursors and with the high triptyl-to-non-triptyl ratios (3.2–4.6; Fig. 2d) that result from hydride transfer and methylation reactions that selectively form and terminate these isomers before they isomerize. Chain termination probabilities ( $\beta$ ; Fig. 3) for 2,3-dimethylbutyl species, however, were higher on FAU (0.20) than BEA (0.07), indicating that the larger voids within FAU channels increase hydride transfer rates to a greater extent than methylation, consistent with the higher selectivities to products smaller than  $C_7$  on FAU than BEA (Fig. 1b). The ratios of the number of  $^{12}\text{C}$ -2,3-dimethyl-2-butene molecules that form  $C_{8+}$  chains and undergo subsequent  $\beta$ -scission to those that form singly labeled triptyls or undergo isomerization or hydride transfer ( $\gamma_{\text{BS}}$ ; determined according to Eq. (2)) are similar on FAU (0.20) and BEA (0.24), reflecting their similar isobutyl selectivities (Fig. 2a).  $C_{8+}$  chains that form and undergo rapid  $\beta$ -scission rapidly terminate as isobutane and cause supra-equilibrium isobutane selectivities in the  $C_4$  fraction on FAU and BEA. We conclude from these isotopic data that the preference for chains with a four-carbon backbone that are smaller than  $C_7$  on FAU compared to BEA reflects hydride transfer rates

that increase to a greater extent than methylation rates with increasing pore size.

In the previous section (Section 3.2.1), we concluded that solvation of transition states within zeolite voids decreases their free energies relative to gas-phase reactants for the conditions where sites remain predominantly vacant. Rate increases that result from enthalpic van der Waals stabilization of transition states are often attenuated by a concomitant decrease in transition-state entropies caused by loss of freedom upon confinement within zeolite pores, as shown for alkane cracking and dehydrogenation on FER, MFI, and MOR [25–27,44]. Furthermore, steric hindrances increase with increasing transition-state size and with decreasing pore size because of entropic penalties imposed by increasing confinement [44]. Thus, replacing BEA channels ( $0.66 \text{ nm} \times 0.67 \text{ nm}$  and  $0.56 \text{ nm} \times 0.57 \text{ nm}$  in diameter [45]) with larger voids in FAU (supercages of 1.3 nm diameter accessed through 0.74 nm windows [45]) leads to smaller losses in entropy for hydride transfer transition states than methylation and isomerization transition states. As a result, the termination probabilities observed on FAU are higher than those on BEA (0.20 vs. 0.07; Fig. 3a). Next, we report homologation rates and selectivities as well as isomerization, termination, and  $C_{8+}$   $\beta$ -scission probabilities on MFI, a medium-pore zeolite, to probe the effects of more severe confinement on the transition states that determine DME homologation selectivities.

### 3.2.3. Effects of confinement within medium pores on $C_1$ homologation chemistry

DME homologation turnover rates were similar (within a factor of 2) on MFI, FAU, and BEA (Table 1b), but product distributions differed significantly among these zeolites (Fig. 1b). The selectivities to  $C_5$ ,  $C_6$ , and  $C_7$  chains were very similar on MFI (Fig. 1b), in sharp contrast to the bimodal distributions to predominantly  $C_4$  and  $C_7$  products observed on large-pore FAU and BEA zeolites. Specifically,  $C_7$  and  $C_4$  selectivities were much lower on MFI (18%  $C_7$  selectivity and 12%  $C_4$  selectivity; Fig. 1b) than on FAU and BEA (23–31%  $C_7$  selectivity and 35–37%  $C_4$  selectivity). Triptyl-to-non-triptyl and isobutyl-to- $n$ -butyl ratios within these products were smaller on MFI (0.1 and 1.5, respectively) than on BEA or FAU (3.2–4.8 triptyl-to-non-triptyl ratios and 4.6–6.3 isobutyl-to- $n$ -butyl ratios; Fig. 2a and d). Isopentyl-to- $n$ -pentyl (19 vs. 32–59; Fig. 2b) and 2,3-dimethylbutyl-to-isoheptyl (0.5 vs. 1.0–1.5; Fig. 2c) isomer ratios were also smaller on MFI. The prevalence of isomers without the four-carbon triptane backbone on MFI zeolites compared to BEA and FAU suggests that chains isomerize more frequently along the methylation path instead of methylating to triptane on the former. Previous isotopic studies [7] have shown that chains lacking this four-carbon backbone are much less likely to terminate than the four-carbon chains that act as triptyl precursors; as a result, these isomerized chains form  $C_{8+}$  chains that undergo  $\beta$ -scission to isobutyl species. The selective formation of molecules without the triptane backbone and the low isobutane selectivities within  $C_4$  hydrocarbons on MFI indicate that the rates of termination of these isomers before methylation are higher on MFI than on BEA or FAU.

Isomerization probabilities ( $\gamma_{\text{sk}}$ ) measured from isotopic  $^{13}\text{C}$ -DME/ $^{12}\text{C}$ -2,3-dimethyl-2-butene experiments were 10-fold larger on MFI (0.06) than on BEA or FAU (0.006–0.008). Chain termination probabilities ( $\beta$ ) from these experiments were larger on MFI (0.17) than on BEA (0.07), but similar to the value measured on FAU (0.20). The combination of these high isomerization and termination probabilities on MFI suggests that MFI terminates some of the isomerized chains before  $\beta$ -scission leading to the high selectivities to products lacking the backbone of triptane on MFI (Fig. 2). These results suggest that confinement within medium pores of MFI influences rates of hydride transfer and isomerization reactions to a greater extent than rates of methylation.

The  $\beta$ -scission probabilities of  $C_{8+}$  chains ( $\gamma_{\beta s}$ ; Fig. 3c) were larger on MFI (0.50) than on BEA (0.24) or FAU (0.20). These higher  $\gamma_{\beta s}$  values indicate that a larger fraction of the chains derived from  $^{12}C$ -2,3-dimethyl-2-butene form  $C_{8+}$  chains that then undergo  $\beta$ -scission on MFI compared with BEA or FAU, apparently because more chains without a four-carbon backbone are prevalent on MFI. This higher  $\gamma_{\beta s}$  value on MFI compared with BEA also indicates that the increase in hydride transfer rates relative to methylation on MFI does not cause the termination of all isomerized chains prior to their methylation to  $C_{8+}$  species followed by  $\beta$ -scission. Previous isotopic studies [7] have shown that the preferred  $C_8$  isomers formed via triptene methylation (2,2,3- and 2,4,4-trimethylpentane) undergo facile  $\beta$ -scission steps via stable tertiary cationic transition states [46] to form isobutyl species that preferentially terminate as isobutane. In contrast to triptene methylation, 2,4-dimethyl-2-pentene methylation preferentially forms 2,3,4-trimethylpentyl isomers that undergo slower  $\beta$ -scission steps (compared to 2,2,3- and 2,4,4-trimethylpentane), because they form isopentene and a secondary propyl cation at the transition state [7,46]; isopentene can then readily re-enter the chain growth path via methylation at much higher rates than isobutene (termination probabilities of 0.21 and 0.54 for isopentyl and isobutyl species, respectively [7]). Thus, we conclude that isobutane selectivities are lower on MFI (isobutyl-to-*n*-butyl ratio = 1.5; Fig. 2a) than on BEA (4.6) and FAU (6.3) despite higher  $\gamma_{\beta s}$  values (0.50 vs. 0.20–0.24) and concentrations of chains without the four-carbon backbone of triptane (Fig. 2), because the  $C_{8+}$  chains on MFI are formed from methylation of molecules without a linear four-carbon backbone and yield higher amounts of isopentene and propene upon  $\beta$ -scission that re-enter chain growth paths.

Termination probabilities ( $\beta$ ; Fig. 3a) for 2,3-dimethylbutyl chains were higher on MFI (0.17) than BEA (0.07), indicating that hydride transfer rates increased to a greater extent than methylation as the larger voids in BEA were replaced with smaller channels in MFI. This apparent benefit from tighter confinement on hydride transfer rates is in contrast to the higher  $\beta$  values on FAU (0.20) compared to BEA (0.07), which indicate an increase in hydride transfer rate with increasing pore size (discussed in Section 3.2.2). This apparent contradiction reflects the difference between the molecular structures of hydrocarbons that are prevalent and serve as hydride donors on MFI and BEA. Previous studies have shown that rates of hydride transfer depend on the strength of the C–H bond in the hydride donor as well as the stability of the carbenium ion formed by the alkoxide acceptor [9,16,47]. Alkenes with tertiary carbon atoms are preferred hydride donors because of their weaker C–H bonds (224 kcal mol<sup>-1</sup> to form tertiary allylic cations from 3-methyl-1-pentene and 2,3-dimethyl-2-butene) relative to those in tertiary alkanes (hydride abstraction energies of 226–230 kcal mol<sup>-1</sup> for isobutane, isopentane, and 2,3-dimethylbutane) and in linear alkanes (247 and 265 kcal mol<sup>-1</sup> for secondary and primary C–H bonds, respectively, in *n*-butane) [8]. Higher isomerization (0.06 vs. 0.006; Fig. 2b) and termination (0.17 vs. 0.07; Fig. 2a) probabilities on MFI than BEA lead to higher concentrations of isohexyl, 2,4- and 2,3-dimethylpentyl, and isoheptyl species (Table 1). Alkanes with these structures can donate hydrides to form alkenes with tertiary allylic C–H bonds that are preferred in hydride transfer reactions. In contrast to MFI, BEA predominantly forms triptyl and isobutyl species, whose alkenes do not possess tertiary allylic C–H bonds, because faster rates of methylation on BEA than MFI react isohexyl, 2,4- and 2,3-dimethylpentyl, and isoheptyl species to  $C_{8+}$  chains that undergo  $\beta$ -scission. The molecules formed on MFI are more effective hydride donors than those formed on BEA because they can participate in multiple hydride transfer steps via stable tertiary carbenium ion transition states and form molecules with weaker C–H bonds. We therefore conclude that the selective increase in hydride

transfer rates compared to methylation for MFI pores, in part, reflects the prevalence of hydrocarbon species (isohexyl, 2,4- and 2,3-dimethylpentyl, and isoheptyl isomers) that are more effective hydride donors than those formed on BEA and FAU (isobutyl and triptyl species).

The observed differences in product selectivities between MFI and BEA or FAU reflect the effects of steric hindrance within pores of different size on the rates of methylation, hydride transfer, and isomerization reactions (also discussed in Section 3.2.2). Severe entropic penalties upon confinement within channels smaller than 12-MR restrict the formation of hydride transfer transition states [44]. By analogy, bulky transition states that mediate bimolecular hydride transfer and methylation steps would be more restricted than smaller ones required in monomolecular isomerization within MFI pores. Thus, rates of isomerization decrease to a lesser extent relative to those of methylation and hydride transfer upon confinement within the smaller pores in MFI compared to BEA and FAU. As a result, selectivities to *n*-butyl, *n*-pentyl, isohexyl, and non-triptyl isomers are higher on MFI than BEA and FAU (Table 1b, Figs. 1b and 2).

#### 4. Conclusions

This study demonstrates that preferential formation of triptane from  $C_1$  precursors via homologation pathways is general to Brønsted acid catalysis, yet rates and selectivities of individual products depend on the location and strength of acid sites. Dimethyl ether (DME) homologation rates and selectivities measured on mesoporous ( $SiO_2-Al_2O_3$  and 5 wt.%  $H_3PW_{12}O_{40}/SiO_2$ ) and zeolitic (BEA, FAU, and MFI) solid acids were used to ascertain the individual effects of acid strength and confinement on hydride transfer, methylation, and isomerization steps within these pathways.

Higher DME turnover rates on 5 wt.%  $H_3PW_{12}O_{40}/SiO_2$  than  $SiO_2-Al_2O_3$  reflect lower activation barriers for all reactions at the strong acid sites of  $H_3PW_{12}O_{40}/SiO_2$ , because charge separation at transition states is less endothermic and the resulting ion-pairs are more stable on stronger acids. Selectivities to *n*-butyl species within  $C_4$  products and isomers within  $C_5-C_7$  products that lack the four-carbon backbone of triptane are higher on 5 wt.%  $H_3PW_{12}O_{40}/SiO_2$  than weaker sites of  $SiO_2-Al_2O_3$  and BEA. Taken together with higher termination and isomerization probabilities measured on  $H_3PW_{12}O_{40}/SiO_2$  from isotopic  $^{13}C$ -DME co-feed experiments, these product selectivities indicate that isomerization and hydride transfer rates preferentially increase over methylation rates on  $H_3PW_{12}O_{40}/SiO_2$ . Diffuse charges of cations at isomerization and hydride transfer transition states are less effective at interacting with the conjugate anion than the localized cations in methylation transition states; as a result, they recover less of the deprotonation energy via electrostatic interactions at the transition state and have stabilities that benefit more from strong acid sites than locally charged methylation transition states.

$SiO_2-Al_2O_3$  has lower DME homologation rates than BEA because methylation, hydride transfer, and isomerization transition states are stabilized relative to extra-zeolite gas-phase reactants by solvation within zeolite channels. Selectivities to  $C_7$  hydrocarbons and specifically triptyl isomers are lower on  $SiO_2-Al_2O_3$  than BEA, indicating that confinement within channels of BEA stabilizes hydride transfer and methylation transition states more effectively than isomerization transition states because an additional reactant is stabilized by van der Waals forces at the transition states of the former.

Rates and selectivities of  $C_1$  homologation products on zeolites with different pore sizes reflect the effects of confinement on the rates of methylation, isomerization, and hydride transfer elementary steps during DME homologation. Termination probabilities are higher on FAU than BEA and cause lower triptane

selectivities. Hydride transfer rates increase more than methylation rates with increasing pore size from BEA to FAU because larger hydride transfer transition states are more sensitive to entropic restrictions caused by smaller pores than methylation transition states. Decreasing void size from BEA and FAU to MFI restricts isomerization transition states less than those for hydride transfer and methylation because medium pores within MFI impose less severe steric constraints on monomolecular isomerization transition states than those for bimolecular hydride transfer and methylation steps. As a result, the product distribution is more uniform and has less triptane precursors on MFI than the bimodal distributions to triptane and isobutane on BEA and FAU.

The results from this study indicate that rates of all reactions are higher on stronger acid sites, but selectivities change based upon the extent to which charge is localized at transition states of the kinetically-relevant elementary reaction. Specifically, the stabilities of diffusely charged cations at transition states are more sensitive to acid strength than localized cations and have activation barriers that are reduced more by stronger acid sites. Solvation of transition states within zeolite voids lowers their free energies relative to extra-zeolite reactants via van der Waals stabilization. The implications of these results for methylation, hydride transfer, and isomerization steps in DME homologation lead us to conclude that weak acid sites and confinement within large pores preferentially stabilize hydride transfer and methylation transition states that preserve the structure of triptane in growing hydrocarbons over isomerization reactions. Thus, isobutane and triptane selectivities are highest on BEA and FAU compared to zeolites with smaller pores (MFI) and mesoporous solid acids with similar ( $\text{SiO}_2\text{-Al}_2\text{O}_3$ ) or stronger (5 wt.%  $\text{H}_3\text{PW}_{12}\text{O}_{40}/\text{SiO}_2$ ) acid sites.

### Acknowledgments

We acknowledge partial financial support from BP p.l.c as part of the Methane Conversion Cooperative Program at the UC-Berkeley and from the Chemical Sciences Division, Office of Basic Energy Sciences, Office of Science, US Department of Energy under Grant No. DE-FG02-03ER15479. We thank Rajamani Gounder for valuable discussions about thermochemical cycles in acid catalysis and about the effects of confinement in zeolite catalysis. We also thank Professor Matthew Neurock (University of Virginia) for useful discussions during the course of this study and Dr. Wei Qi for the synthesis of 5 wt.%  $\text{H}_3\text{PW}_{12}\text{O}_{40}/\text{SiO}_2$  and the titration data on this sample.

### Appendix A. Supplementary material

Supplementary data associated with this article can be found, in the online version, at doi:10.1016/j.jcat.2011.09.007.

### References

- [1] J.E. Bercaw, P.L. Diaconescu, R.H. Grubbs, N. Hazari, R.D. Kay, J.A. Labinger, P. Mehrkhodavandi, G.E. Morris, G.J. Sunley, P. Vagner, *Inorg. Chem.* 46 (2007) 11371.
- [2] J.E. Bercaw, P.L. Diaconescu, R.H. Grubbs, R.D. Kay, S. Kitching, J.A. Labinger, X. Li, P. Mehrkhodavandi, G.E. Morris, G.J. Sunley, P. Vagner, *J. Org. Chem.* 71 (2006) 8907.
- [3] J.E. Bercaw, R.H. Grubbs, N. Hazari, J.A. Labinger, X.W. Li, *Chem. Commun.* (2007) 2974.
- [4] J.E. Bercaw, N. Hazari, J.A. Labinger, V.J. Scott, G.J. Sunley, *J. Am. Chem. Soc.* 130 (2008) 11988.
- [5] N. Hazari, J.A. Labinger, V.J. Scott, *J. Catal.* 263 (2009) 266.
- [6] J.H. Ahn, B. Temel, E. Iglesia, *Angew. Chem. Int. Ed.* 48 (2009) 3814.
- [7] D.A. Simonetti, J.H. Ahn, E. Iglesia, *J. Catal.* 277 (2011) 173.
- [8] D.H. Aue, M.T. Bowers, in: M.T. Bowers (Ed.), *Gas-Phase Ion Chemistry*, vol. 2, Academic Press, New York, 1979 (Chapter 9).
- [9] M. Boronat, P. Viruela, A. Corma, *J. Phys. Chem. A* 102 (1998) 9863.
- [10] M.J. Janik, R.J. Davis, M. Neurock, *Catal. Today* 105 (2005) 134.
- [11] M. Bjorgen, U. Olsbye, S. Svelle, S. Kolboe, *Catal. Lett.* 93 (2004) 37.
- [12] R.J. Pellet, C.S. Blackwell, J.A. Rabo, *J. Catal.* 114 (1988) 71.
- [13] G.W. Skeels, D.W. Breck, *Proceedings of the Sixth International Zeolite Conference*, 1984, p. 87.
- [14] R.T. Carr, M. Neurock, E. Iglesia, *J. Catal.* 278 (2011) 78.
- [15] G.L. Price, E. Iglesia, *Ind. Eng. Chem. Res.* 28 (1989) 839.
- [16] D.A. Simonetti, J.H. Ahn, E. Iglesia, *Chem. Catal. Chem.* 3 (2011) 704.
- [17] W. Wang, A. Buchholz, M. Seiler, M. Hunger, *J. Am. Chem. Soc.* 125 (2003) 15260.
- [18] M. Brandle, J. Sauer, *J. Am. Chem. Soc.* 120 (1998) 1556.
- [19] J. Macht, M.J. Janik, M. Neurock, E. Iglesia, *Angew. Chem. Int. Ed.* 46 (2007) 7864.
- [20] J. Macht, R.T. Carr, E. Iglesia, *J. Catal.* 264 (2009) 54.
- [21] C. Lo, B.L. Trout, *J. Catal.* 227 (2004) 77.
- [22] J. Macht, R.T. Carr, E. Iglesia, *J. Am. Chem. Soc.* 131 (2009) 6554.
- [23] J. Macht, M.J. Janik, M. Neurock, E. Iglesia, *J. Am. Chem. Soc.* 130 (2008) 10369.
- [24] M. Janik, J. Macht, E. Iglesia, M. Neurock, *J. Phys. Chem.* 113 (2009) 1872.
- [25] A. Bhan, R. Gounder, J. Macht, E. Iglesia, *J. Catal.* 253 (2008) 221.
- [26] R. Gounder, E. Iglesia, *J. Am. Chem. Soc.* 131 (2009) 1958.
- [27] R. Gounder, E. Iglesia, *Angew. Chem. Int. Ed.* 49 (2010) 808.
- [28] S. Svelle, C. Tuma, X. Rozanska, T. Kerber, J. Sauer, *J. Am. Chem. Soc.* 131 (2009) 816.
- [29] M.A. Natal-Santiago, R. Alcalá, J.A. Dumesic, *J. Catal.* 181 (1999) 124.
- [30] S. Svelle, B. Arstad, S. Kolboe, O. Swang, *J. Phys. Chem. B* 107 (2003) 9281.
- [31] M.J. Janik, R.J. Davis, M. Neurock, *J. Catal.* 244 (2006) 65.
- [32] M.V. Frash, V.B. Kazanzky, A.M. Rigby, R.A. van-Santen, *J. Phys. Chem. B* 101 (1997) 5346.
- [33] F. Eder, J.A. Lercher, *Zeolites* 18 (1997) 75.
- [34] F. Eder, M. Stockenhuber, J.A. Lercher, *J. Phys. Chem. B* 101 (1997) 5414.
- [35] S. Savitz, F. Siperstein, R.J. Gorte, A.L. Myers, *J. Phys. Chem. B* 102 (1998) 6865.
- [36] J. Bandiera, M. Dufaux, Y.B. Taarit, *Appl. Catal. A* 148 (1997) 283.
- [37] J. Bandiera, Y.B. Taarit, *Appl. Catal.* 62 (1990) 309.
- [38] W.O. Haag, *Stud. Surf. Sci. Catal.* 84 (1994) 1375.
- [39] T.F. Narbeshuber, A. Brait, K. Seshan, J.A. Lercher, *J. Catal.* 172 (1997) 127.
- [40] T.F. Narbeshuber, H. Vinek, J.A. Lercher, *J. Catal.* 157 (1995) 388.
- [41] X. Wang, H. Carabineiro, F. Lemons, M.A. Lemons, F.R. Ribeiro, *J. Mol. Catal. A – Chem.* 216 (2004) 131.
- [42] J. Wei, *Chem. Eng. Sci.* 51 (1996) 2995.
- [43] B. Xu, C. Sievers, S.B. Hong, R. Prins, J.A.v. Bokhoven, *J. Catal.* (2006) 163.
- [44] B.G. Anderson, R.R. Schumacher, R. van-Duren, A.P. Singh, R.A. van-Santen, *J. Mol. Catal. A – Chem.* 181 (2002) 291.
- [45] C. Baerlocher, W.M. Meier, O.H. Olson, *Atlas of Zeolite Framework types*, 2001.
- [46] J.S. Buchanan, J.G. Santiesteban, W.O. Haag, *J. Catal.* 158 (1996) 279.
- [47] M. Boronat, P. Viruela, A. Corma, *J. Phys. Chem. B* 103 (1999) 7809.